

# $\gamma$ -ray anisotropies from dark matter in the Milky Way: the role of the radial distribution

F. Calore<sup>1</sup>, V. De Romeri<sup>2</sup>, M. Di Mauro<sup>3,4,5</sup>, F. Donato<sup>3,4</sup>, J. Herpich<sup>6</sup>, A.V. Macciò<sup>6</sup>, L. Maccione<sup>7,8</sup>

<sup>1</sup> GRAPPA Institute, University of Amsterdam, Science Park 904, 1090 GL Amsterdam, The Netherlands

<sup>2</sup> Laboratoire de Physique Corpusculaire, CNRS/IN2P3 - UMR 6533, Campus des Cézeaux, 24 Av. des Landais, F-63177 Aubièze Cedex, France

<sup>3</sup> Dipartimento di Fisica, Università di Torino, via Giuria 1, I-10125 Torino, Italy

<sup>4</sup> INFN, Sezione di Torino, I-10125 Torino, Italy

<sup>5</sup> Laboratoire d'Annecy-le-Vieux de Physique Théorique (LAPTh), Univ. de Savoie, CNRS, B.P.110, Annecy-le-Vieux F-74941, France

<sup>6</sup> Max-Planck-Institut für Astronomie, Königstuhl 17, 69117 Heidelberg, Germany

<sup>7</sup> Ludwig-Maximilians-Universität, Theresienstraße 37, D-80333 München, Germany and

<sup>8</sup> Max-Planck-Institut für Physik (Werner Heisenberg Institut), Föhringer Ring 6, D-80805 München, Germany

LAPTH-009/14, PCCF RI 14-03

## ABSTRACT

The annihilation of dark matter particles in the halo of galaxies may end up into  $\gamma$ -rays, which travel almost unperturbed till to their detection at Earth. This annihilation signal can exhibit an anisotropic behavior quantified by the angular power spectrum, whose properties strongly depend on the dark matter distribution and its clumpiness. We use high resolution pure dark matter N-body simulations to quantify the contribution of different components (main halo and satellites) to the global signal as a function of the analytical profile adopted to describe the numerical results. We find that the smooth main halo dominates the angular power spectrum of the  $\gamma$ -ray signal up to quite large multipoles, where the sub-haloes anisotropy signal starts to emerge, but the transition multipole strongly depends on the assumed radial profile. The extrapolation down to radii not resolved by current numerical simulations can affect both the normalization *and* the shape of the  $\gamma$ -ray angular power spectrum. For the sub-haloes described by an asymptotically cored dark matter distribution, the angular power spectrum shows an overall smaller normalization and a flattening at high multipoles. Our results show the criticality of the dark matter density profile shape in  $\gamma$ -ray anisotropy searches, and evaluate quantitatively the intrinsic errors occurring when extrapolating the dark matter radial profiles down to spatial scales not yet explored by numerical simulations.

**Key words:** cosmology: formation – galaxies: methods: numerical

## 1 INTRODUCTION

One of the most reliable solutions to the missing mass in the Universe implies that it is constituted by Weakly Interacting Massive Particles (WIMPs), clustered in galaxies as dark haloes. The astrophysical evidence of these particle dark matter (DM) candidates can be explored by direct as well as indirect detection techniques. In the latter case, the idea is that WIMP DM may annihilate in pairs and produce charged particles and  $\gamma$ -rays, detectable as rare components in cosmic rays. Differently from the charged cosmic rays, the flux of  $\gamma$ -rays arriving at the Earth is not deflected by magnetic fields and traces back directly to its sources. The search for DM through  $\gamma$ -rays is therefore a preferential

tool for exploiting the properties of its spatial distribution (Bringmann & Weniger (2012) and refs. therein).

The excellent performances of the Large Area Telescope (LAT) on the Fermi  $\gamma$ -ray space Telescope (*Fermi*) have let the exploration for a DM component in the Milky Way, in extragalactic nearby objects, as well as in cosmological structures (Ackermann et al. 2012a, 2010b,a; Abdo et al. 2010; Ackermann et al. 2011). At high galactic latitudes, a faint  $\gamma$ -ray irreducible emission has been measured, and shown to be isotropic at a high degree (Ackermann et al. 2012b). The *Fermi*-LAT has already reported the detection of a non-zero angular power spectrum (APS) above the noise level in the multipole range  $\ell \sim 155 \div 504$ , corresponding to an angular scale  $\lesssim 2^\circ$ , with a significance ranging from  $5.3\sigma$

between 2 and 5 GeV to  $0.8\sigma$  between 10.4 and 50 GeV (Ackermann et al. 2012b).

Different predictions for the APS have been proposed for various populations of unresolved sources, both of astrophysical (Cuoco et al. 2012; Siegal-Gaskins et al. 2011; Harding & Abazajian 2012) and of DM origin (Fornasa et al. 2009, 2013; Ando & Komatsu 2013; Siegal-Gaskins 2008). Since it is expected that the statistical properties of the DM distribution in galactic and extragalactic space are different from those of standard astrophysical objects, the study of the APS ascribable to DM sources may be an important signature worth to be explored.

The intensity of the  $\gamma$ -ray signal depends on a particle physics term - describing the strength and the energy spectrum of the annihilation - and on the DM density in collapsed structures. While the first factor includes the details of the assumed particle physics model for the WIMPs, the second one has an astrophysical origin and it is usually modeled according to the results of cosmological collisionless simulations, generally predicting a steepening of the DM profile in the inner parts of the resolved halos (e.g. Springel et al. (2008); Diemand et al. (2008) and references therein). Therefore, the most likely detectable targets have been identified with especially dense regions such as the galactic center (Gomez-Vargas et al. 2013; Ackermann et al. 2013b), and the center of any DM sub-structure orbiting in the Milky Way halo, like faint and ultra faint dwarf galaxies (Walker et al. 2011; Ackermann et al. 2013a).

The APS gives the measure of a signal correlation between two angular scales, and, in turns, between two spatial scales. For a source located at the galactic center, like the main halo of the Milky Way, the APS at multipoles, for example,  $\ell > 500$  probes the DM distribution at  $R < \pi/500 \cdot 8.5 \text{ kpc} \sim 40 \text{ pc}$ . The study of the APS at  $l \gtrsim 500$  requires therefore to know the DM profile at scales much below the resolution ( $\sim 200 \text{ pc}$ ) of current state of the art numerical simulations for structure formation (Springel et al. 2008; Diemand et al. 2008; Stadel et al. 2009). Several profile parameterizations provide excellent fits to the DM distribution of simulated halos (Navarro et al. 1996, 2004; Graham et al. 2006; Macciò et al. 2008; Stadel et al. 2009). However, when extrapolated below the resolution limit of cosmological simulations, different profiles predict very different central densities.

In this paper we discuss in detail these points when applied to the anisotropy in the  $\gamma$ -ray flux from DM annihilation, namely: i) the intrinsic uncertainty due to the extrapolation to short distances of the DM distribution determined from numerical simulations; ii) the different signatures in the APS in connection with the various density profiles (cored and cuspy).

## 2 THE $\gamma$ -RAY FLUX FROM DM ANNIHILATION

The  $\gamma$ -ray flux  $d\Phi_\gamma/dE_\gamma$  from DM annihilating particles is defined as the number of photons collected by a detector per unit of time, area, solid angle and observed energy  $E_\gamma$ . When looking at the direction  $\psi$  and  $\theta$  (longitude and latitude in Galactic coordinates, respectively) in the sky, by an

experiment with spatial resolution  $\alpha$  and under a solid angle  $\Delta\Omega = 2\pi(1 - \cos \alpha)$ , it may be expressed as:

$$\frac{d\Phi_\gamma}{dE_\gamma}(E_\gamma, \psi, \theta, \Delta\Omega) = \quad (1)$$

$$\frac{1}{4\pi} \frac{\langle \sigma_{\text{ann}} v \rangle}{2m_\chi^2} \cdot \sum_i B_i \cdot \frac{dN_\gamma^i}{dE_\gamma} \int_0^{\Delta\Omega} d\Omega \int_{\text{l.o.s.}} \rho^2(r(s, \psi, \theta)) ds.$$

Here  $m_\chi$  is the mass of the DM particle and  $\langle \sigma_{\text{ann}} v \rangle$  is the annihilation cross section times the relative velocity averaged over the DM velocity distribution.  $B_i$  is the branching ratio into the final state  $i$  and  $dN_\gamma^i/dE_\gamma$  is the photon spectrum per annihilation (which depends on the annihilation channels). The sum is in principle performed over all the annihilation channels. The last term in Eq. 1 contains the (squared) DM density  $\rho(r)$  ( $r$  being the galactocentric distance) integrated along a distance  $s$  from the Earth in the direction along the line of sight (l.o.s), and in the observational cone of solid angle  $\Delta\Omega$ . In the following of our analysis, if not differently stated, we will choose as representative the annihilation into the  $b\bar{b}$  quark channel with  $B_{b\bar{b}}=1$ , and fix  $m_\chi=200 \text{ GeV}$ ,  $E_\gamma=4 \text{ GeV}$  and  $\langle \sigma_{\text{ann}} v \rangle = 3 \cdot 10^{-26} \text{ cm}^3 \text{ s}^{-1}$ . We remark that this choice does not affect our main results, since throughout the analysis the particle physics factor may be considered as a mere normalization of the APS.

### 2.1 Simulations for the DM spatial distribution

The simulations presented in this paper are the pure DM N-body counterparts of the MaGICC (Making Galaxies in a Cosmological Context) simulations suite (Stinson et al. (2013); Di Cintio et al. (2014) for more details). The galaxy we discuss in details is g15784, which has a virial mass of  $1.48 \times 10^{12} M_\odot$ , very close to the mass of the Milky Way (Xue et al. 2008). We resolve a total of 27 substructures in the simulation in a mass range of  $10^{8.6} - 10^{9.6} M_\odot$ .

For determining the  $\gamma$ -ray emission, as clear from Eq. 1, a special role is deserved to the radial density profile of the DM halo  $\rho(r)$ , with particular attention to the central region. This is true both for the central smooth halo as well as for the sub-structures.

We have decided to use three different analytical profiles to describe the DM distribution in our simulation: the widely used Navarro, Frenk & White profile (Navarro et al. (1997), NFW hereafter), the Einasto profile (Einasto (1965); Kutuzov & Einasto (1968); Einasto (1969), Ein hereafter) which has been shown to be a better representation of the DM distribution in simulated haloes (Dutton & Macciò (2014)), and the profile suggested by Moore and Stadel (Stadel et al. (2009), MS hereafter):

$$\rho(r) = \rho_0 \left[ \left( \frac{r}{R_c} \right) \left( 1 + \frac{r}{R_c} \right)^2 \right]^{-1} \quad (\text{NFW}) \quad (2)$$

$$\rho(r) = \rho_0 \exp \left( -\frac{2}{\alpha_E} \left[ \left( \frac{r}{R_s} \right)^{\alpha_E} - 1 \right] \right) \quad (\text{Ein}) \quad (3)$$

$$\rho(r) = \rho_0 \exp \left( -\lambda \left[ \ln \left( 1 + \frac{r}{R_\lambda} \right) \right]^2 \right) \quad (\text{MS}) \quad (4)$$

where  $\rho_0$ ,  $R_c$ ,  $R_s$ ,  $\alpha_E$ ,  $\lambda$ ,  $R_\lambda$  are the free parameters in the different analytic profiles. In this latest parameterization the

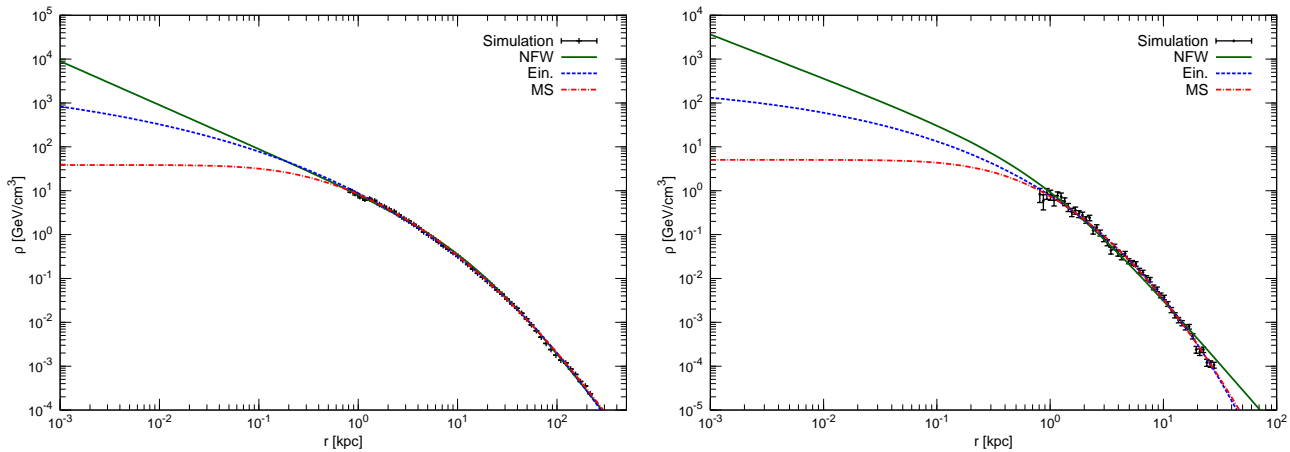


**Figure 1.** DM density profile as a function of the radius  $r$  from the center of the halo. The left panel displays the results for the main halo, the right panel for a sub-halo resolved in the simulation g15784. The simulation data are shown by black dots, while the different profiles described in Eqs. 2 (NFW), 3 (Ein), 4 (MS), and their extrapolation to smaller scales, are shown by the red solid, blue dotted and green dot-dashed lines, respectively.

density profile is linear down to a scale  $R_\lambda$ , beyond which it approaches the central maximum density  $\rho_0$  as  $r \rightarrow 0$ . This fitting function is extremely flexible and makes possible to reproduce at the same time both cuspy and cored profiles (e.g. Macciò et al. (2012)). The results of the different fits to the DM distribution are shown in Fig. 1. We notice that throughout this work the main halo is intended to be the total DM halo. In the left panel, it is clear that all the different profiles described above provide a very good fit to the numerical radial density on the whole range probed by the simulation (0.8-250 kpc). On the other hand, they dramatically diverge when extrapolated beyond the resolution limit of the simulation. The MS profile predicts an extended core below 50-100 pc, while the Einasto and NFW profiles both imply an increased density towards the center, even though with a quite different slope. As a result, the central DM halo density at the  $\approx 10$  pc scales - the most relevant scale for  $\gamma$ -rays production - differs by a factor of fifty between the two most extreme cases (MS and NFW) and by an order of magnitude between Einasto and MS radial profiles. Similar results may be drawn for a sub-halo resolved in the simulation g15784 and fitted with the same functions (Fig. 1, right panel). In this case, the NFW density profile shows some tension also with data at larger radii. The central DM halo density at about 10 pc differs by more than two orders of magnitude between the two most extreme cases (MS and NFW) and by an order of magnitude between the two cuspy profiles (Einasto and NFW).

These simple plots show how problematic (and dangerous) it is the extrapolation of cosmological N-body simulations results on very small spatial scales. As we will see in the rest of the paper, this extrapolation has profound effects on the predicted  $\gamma$ -ray DM signal and the relative contribution of different components like the central halo and its satellites to the APS.

## 2.2 The angular power spectrum of $\gamma$ -ray anisotropies.

The intensity APS  $C_\ell$  of a map  $I(\Psi)$ , where  $\Psi$  is a direction in the sky, is given by the coefficients

$$C_\ell = \frac{1}{2\ell + 1} \sum_{|m| < \ell} |a_{\ell m}|^2, \quad (5)$$

with the  $a_{\ell m}$  determined by expanding the sky map in spherical harmonics, after subtracting the average value of the intensity over the region of the sky considered:

$$I(\Psi) = \frac{d\Phi}{dE}(\Psi) - \langle \frac{d\Phi}{dE}(\Psi) \rangle = \sum_{\ell=0}^{\infty} \sum_{m=-\ell}^{m=\ell} a_{\ell m} Y_{\ell m}(\Psi). \quad (6)$$

The  $\gamma$ -ray intensity maps and their power spectra have been generated by using the HEALPix software (Górski et al. 2005). Depending on the parameter order  $k$ , the number of pixels of the map is  $N_{\text{pixel}} = 12 \cdot 2^{2k}$ . Hence, the solid angle of one pixel of the map is  $\Delta\Omega = 4\pi/N_{\text{pixel}}$ . We fix  $k=13$ , so that  $\Delta\Omega = 1.56 \cdot 10^{-8}$  sr for a corresponding scale of about 1 pc, except for the results of the Monte Carlo simulation where the order parameter is fixed to  $k=9$  for  $\Delta\Omega = 4 \cdot 10^{-6}$  sr. The maximum multipole number  $l_{\text{max}}$  compatible with a fixed map resolution is  $l_{\text{max}} \sim 2 \cdot 2^k$ , therefore  $\sim 1.6 \cdot 10^4$  (1024) for  $k=13$  ( $k=9$ ) (Górski et al. 2005).

## 3 RESULTS

We have computed the space distribution of the  $\gamma$ -ray emission from DM annihilation based on the g15784 halo simulation, described in Sect. 2.1. The resulting simulated sky is illustrated in Fig. 2, where we plot the  $\gamma$ -ray emission maps at  $E_\gamma=4$  GeV, from a DM halo composed by WIMPs with  $m_\chi=200$  GeV (see Sect. 2 for details). In the left panels, the main halo and the sub-haloes are interpreted with the Einasto DM spatial distribution in Eq. 3, while the right panels show the same halo when described by the MS  $\rho(r)$  (Eq. 4). The color code refers to the intensity of the map and goes from blue to red with increasing flux, with different scales for the main

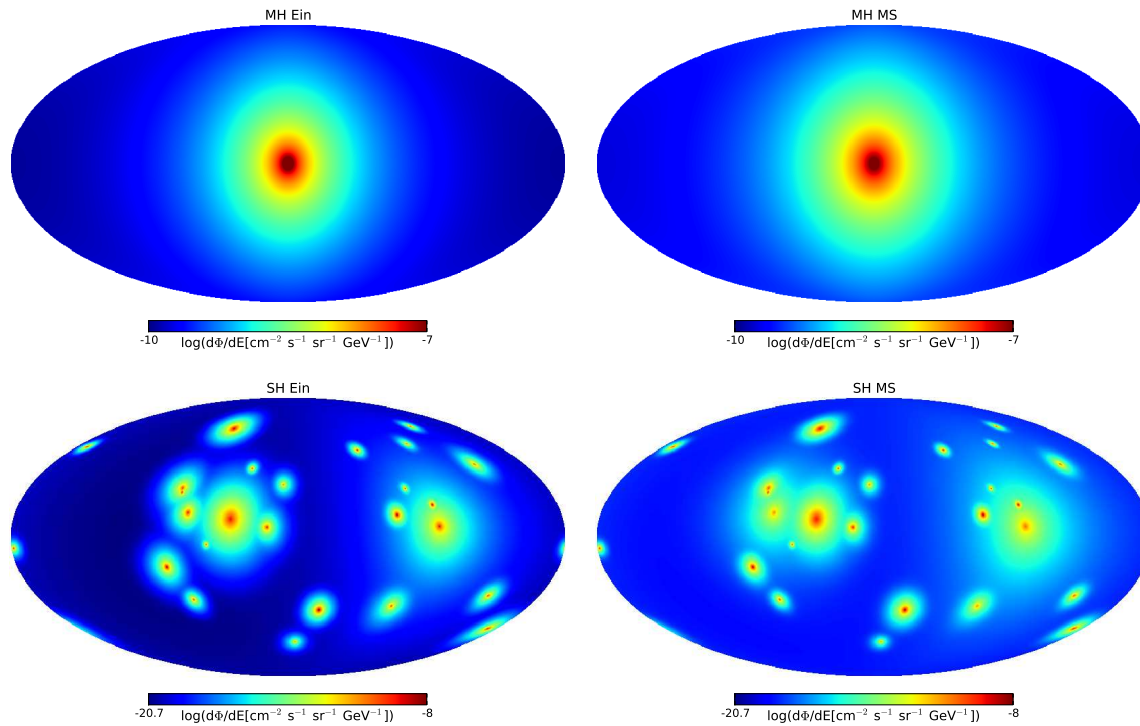


**Figure 2.** All-sky maps of the  $\gamma$ -ray emission at  $E_\gamma=4$  GeV, from the annihilation of  $m_\chi=200$  GeV DM in the simulated galactic halo g15784. In the left (right) panels the main smooth halo (MH, upper plot) and sub-haloes (SH, lower plots) are interpreted with the Einasto (MS) radial density profile, Eq. 3 (Eq. 4).

halo and the sub-structures. The emission from the smooth component (top panels), as expected, extends at larger radii for the MS parameterization, while it is more concentrated in the center for the Einasto profile, given the steeper behavior towards the center of the galaxy. The same argument applies to each sub-halo of the simulation: when interpreted as distributed according to the Einasto profile, the most of the  $\gamma$ -ray emission of each sub-halo mainly originates from the very center of the sub-structure, while in the case of MS the emission is distributed over a larger region, rightly because the core of the DM profile is more extended.

We have calculated the intensity APS for the all-sky  $\gamma$ -ray maps of the simulated galaxy, for both the smooth halo and the resolved sub-structures. The  $\gamma$ -ray intensity in a given direction is obtained by piling up the contribution from all sub-haloes encountered along the l.o.s., up to a distance of 500 kpc. The results are shown in Fig. 3, where the intensity APS for the main halo and the sub-haloes is described, alternatively, by the parameterizations of Eqs. 3 and 4. The figure has been obtained setting the HEALPix resolution  $k=13$ . The halo, when interpreted in terms of the peaked Einasto profile, yields much more power at small radial scales (high  $l$ ), and this is true for both the smooth halo and the sub-haloes. The two profiles give comparable APS only for  $l \lesssim 10$ , while at  $l=100$  the Einasto APS is about two orders of magnitude higher than the MS one. At very small scales, such as  $l=1000$  or, equivalently  $\sim 30$  pc, the main halo within the MS profile does not contribute any longer to the anisotropy of the sky, while the Einasto profile still provides a sizable APS (about eight orders of magnitude above the MS contribution). For illustrative purposes,

we also plot the intensity APS for the main smooth halo interpreted in terms of a NFW  $\rho(r)$  (which indeed fails to properly fit the simulated sub-haloes). The implied APS is very high at all scales, even with respect to the Einasto modeling. At  $l=1000$ , the cuspsiness of the NFW profile gives an APS 100 times more intense than for the Einasto model.

As to the sub-haloes contribution, again the APS is much milder in the case of the cored MS profile than the Einasto one. At  $l=1000$ , the APS for the two models differs by more than two orders of magnitude. In the case of Einasto profile, the emission from the clumps is very anisotropic and similar to the emission of a point-source population, while in the case of the cored MS profile the  $\gamma$ -ray flux from each halo is more smoothly distributed over its radial dimension. The result is that the APS of the sub-structures for the Einasto profile is more concentrated in the center, i.e. higher in normalization, with respect to the MS one since the clumps, appearing more as point-like, inject more power at all scales. This can also be understood by inspecting the all-sky  $\gamma$ -ray maps (see Figs. 2): comparing the Einasto and MS parameterization it is clear that the emission from the MS profile is more isotropic on the sky than the Einasto one. The sub-haloes APS trend for the Einasto and MS profiles is very similar up to  $l \simeq 100$ , the former being stronger by a factor 15-20. Both curves grow proportionally to  $l^2$  as typically expected for a population of point-like sources. For higher multipoles, the APS starts to flatten because the central part of the sub-haloes starts to be resolved (Ando 2009). This property is striking for the MS case, for which the sub-haloes  $C_l$  spectrum flattens around  $l \simeq 400$  and then decreases significantly. Indeed the core of the sub-structures

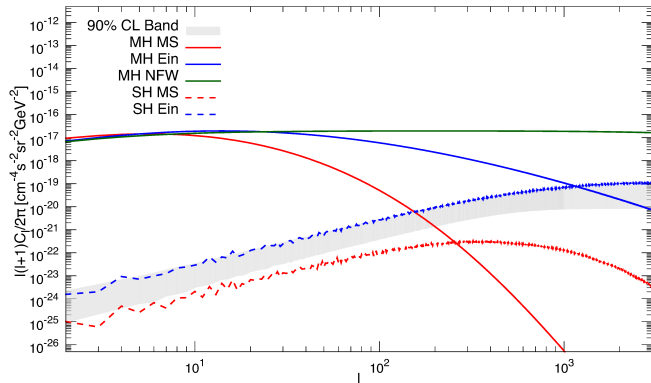


**Figure 3.** Intensity APS for the simulated halo g15784, as a function of the multipole number. The solid blue (red) line describes the smooth halo according to the Einasto (MS) profile, while the dotted lines are for the corresponding sub-haloes contribution. The green solid line displays results for an NFW profile fitting the smooth halo. The grey band refers to the 90% CL uncertainty related to the orientation of the sub-haloes of the g15784 simulation.

is, on average,  $\sim 1.5$  kpc which corresponds to a multipole  $\ell \sim 300$  for a source at  $\sim 200$  kpc as it is the average distance of the clumps in the g15784 simulation. The flattening for the Einasto case is much milder and occurs at smaller scales because within this profile the core is less pronounced.

As clear from Fig. 3, the APS yielded by the Einasto profile is dominated by the smooth halo up to  $l \simeq 1000$ . At variance, the same galactic halo interpreted in terms of the MS radial profile yields an APS for the sub-haloes which dominates over the smooth halo for  $l \gtrsim 250$ . In principle, future observations of the shape of the APS ascribable to DM, will allow to explore the distribution of galactic DM at scales smaller than the resolution of  $N$ -body simulations. The study of high-multipoles anisotropies - achievable by the next generation of Cherenkov telescopes such as CTA (Ripken et al. 2014) - might help in the debate about the real shape of the DM distribution in the center of the galaxies, and in particular of the Milky Way. We also notice that the computation of the APS relies on the full  $\gamma$ -ray sky maps and, thus, does not mask any part of the sky that would be required in order to compare our prediction with the *Fermi*-LAT results.

In order to verify the role of the orientation of the sub-haloes on the APS of the g15784 simulation, we have generated about 850 Monte Carlo realisations in which we have randomly assigned the latitude and longitude of each original sub-halo, while keeping fixed the distance. The corresponding 90% confidence level uncertainty band for the Einasto parameterization of the sub-haloes, is shown by the grey band in Fig. 3 (we have verified that the simulated  $C_\ell$  distribute normally). The fact that the APS of the g15784 simulation stands in the upper edge of the band is somewhat expected, since sub-haloes in a DM only simulation are usually distributed anisotropically and are preferentially located along the major axes of the triaxial mass distributions of their hosts (e.g Zentner et al. 2005). By randomising their positions we tend to go towards a more isotropic distribution that differs from the original simulated one.

Finally, we have inspected the effect of sub-haloes

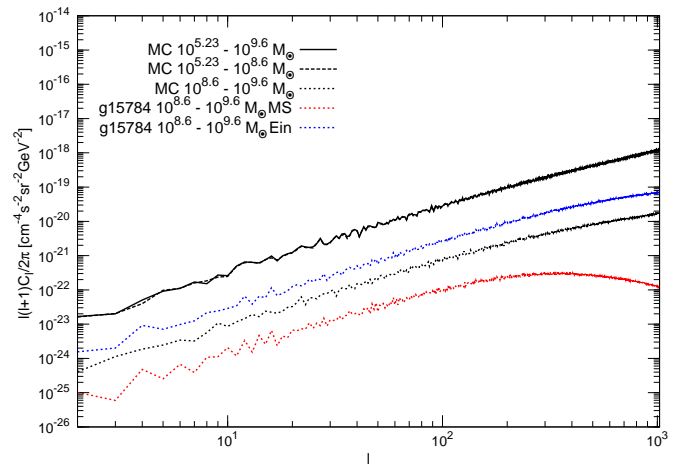


**Figure 4.** Intensity APS computed for the sub-haloes resolved by the g15784 simulation, when the DM density profile is interpreted with an Einasto (upper blues solid line) or a MS profile (lower red solid line). We also plot the results from a Monte Carlo (MC) realization based on Aquarius Aq-A-1 simulation, for sub-haloes having masses from  $10^{5.23} - 10^{9.6} M_\odot$  (black solid line),  $10^{5.23} - 10^{8.6} M_\odot$  (black dashed line) and  $10^{8.6} - 10^{9.6} M_\odot$  (black dotted line).

smaller than the ones obtained in the present cosmological simulation. Fig. 4 depicts the APS computed for the set of sub-haloes resolved by the g15784 simulation (same as in Fig. 3), again interpreted both within Einasto and MS DM profiles. In addition, we also report the APS generated by a realisation of our Monte Carlo simulation based on the Aquarius Aq-A-1 results (Springel et al. 2008). For this purpose, we used the spatial, mass and concentration distributions for the clumps population given by Pieri et al. (2011), and we assume the DM profile in both the main halo and the sub-haloes to follow the Einasto parameterization with  $\alpha_E = 0.18$ . For an easier comparison, we show the APS for different mass ranges:  $10^{5.23} - 10^{9.6} M_\odot$ ,  $10^{5.23} - 10^{8.6} M_\odot$  and  $10^{8.6} - 10^{9.6} M_\odot$ . The more massive haloes lead to the flattening of the APS at large multipoles, as expected, while the contribution of the sub-structures lighter than  $10^{8.6} M_\odot$  is slightly more Poisson-like, and dominates the total APS, which results to be more intense because of this additional component. Given the uncertainties in extrapolating the mass-concentration relation beyond the resolution of the simulations (Ludlow et al. (2013); Sanchez-Conde & Prada (2013)), we decided not to consider masses smaller than the Aq-A-1 resolution ( $\sim 10^5 M_\odot$ ).

In the present analysis we have not included any contribution from DM in extragalactic structures. As discussed in Fornasa et al. (2013) (see also Sefusatti et al. (2014)), the contribution from extragalactic DM halos and sub-halos that are not resolved by  $N$ -body simulations leads to about two orders of magnitude uncertainty on the predicted level of the extragalactic energy spectrum, which may result as the dominant or the sub-dominant component of the total energy spectrum. Similarly, the intensity APS can receive a significant or a negligible contribution from extragalactic (sub)structures.

#### 4 CONCLUSIONS

We have calculated the intensity APS of the  $\gamma$ -ray flux from DM annihilation in the halo of a Milky Way like galaxy, employing the original results from recent numerical simulations of structure formation, which predict the DM phase space and its clustering into sub-haloes. The simulated galactic halo and its sub-haloes can be equally well interpreted in terms of a peaked Einasto as well as an asymptotically cored MS radial dark matter profile.

We show here that the different parameterizations for the DM density distribution leads to very different predictions for the  $\gamma$ -ray intensity APS. The DM halo and sub-haloes, when interpreted in terms of the peaked Einasto profile, yield much higher APS at small radial scales (high  $l$ ) than the cored MS  $\rho(r)$ . The two profiles give comparable APS for the main halo only for  $l \lesssim 10$ , while at  $l=100$  the Einasto APS is about two orders of magnitude higher than the MS one. At very small scales,  $l \simeq 1000$ , the main halo within the MS profile does not contribute any longer to the anisotropy of the sky, while the Einasto profile still provides a sizable APS (about eight orders of magnitude above the MS contribution). We have also proven that the sub-haloes APS is significantly lower for the MS case. Indeed, the APS of the sub-structures described by the Einasto profile is higher than the MS one since the sub-haloes, appearing as point-like sources, inject more angular power at almost all scales.

Our results demonstrate that the extrapolation of the radial DM profile down to radii not proven by cosmological simulations is specially dangerous when dealing with the search for anisotropies in the  $\gamma$ -ray emission. The results for the APS at high multipoles may differ by huge amounts by a mere re-interpretation of the simulated haloes with a different DM radial density distribution. Also, depending of the assumed profile, it may occur that the sub-haloes give a peculiar signature in the APS or, at variance, that the main halo dominates at all multipoles the  $\gamma$ -ray emission. In the latter case, the APS signature for DM annihilating in the galactic halo is significantly weakened.

As a final comment, we underline the caution in adopting extrapolated DM profiles when dealing with anisotropy searches, and emphasize the need for a better knowledge of the distribution of the DM in its clustered structures, especially taking into account the possible effects of baryonic matter (e.g. Macciò et al. (2012); Di Cintio et al. (2014)). On the other hand,  $\gamma$ -ray anisotropy analysis will turn out to be crucial for probing the spatial DM distribution in the galaxy. Indeed, high multipoles measurements will probe scales well beyond the simulations' resolution and will help in discriminating the DM profile at very small radii.

#### ACKNOWLEDGMENTS

We acknowledge E. Borriello for the discussions during the first stages of this work and H. Zechlin for a careful reading of the manuscript. Moreover, we are grateful to the anonymous referee for having suggested us interesting developments of the discussion. F.C. acknowledges support from the German Research Foundation (DFG) through grant BR 3954/1-1 and, for the latest stage of

this work, from the European Research Council through the ERC starting grant WIMPs Kairos, P.I. G. Bertone. F.C. is grateful to S. Ando, T. Bringmann, D. Horns and H.S. Zechlin for useful and stimulating discussions. V.D.R. acknowledges support from the EU Network grant UNILHC PITN-GA-2009-237920 (Universidad de Valencia) for the first stages of this work and from the EU FP7 ITN INVISIBLES (Marie Curie Actions, PITN-GA-2011-289442). A.V.M. acknowledges the support from the Sonderforschungsbereich SFB 881 "the Milky Way System" (sub-project A1) of the German Research Foundation (DFG). J.H. received funding from the European Research Council under the European Union's Seventh Framework Programme (FP 7) ERC Grant Agreement n. [321035]. For the analysis we used the "Amiga Halo Finder" (AHF, [popia.ft.uam.es/AHF/](http://popia.ft.uam.es/AHF/)) for identifying halos and the PYNBODY package ([github.com/pynbody/pynbody/](https://github.com/pynbody/pynbody/)) for their analysis.

#### REFERENCES

- Abdo A., et al., 2010, JCAP, 1004, 014  
 Ackermann M., et al., 2010a, JCAP, 5, 25  
 Ackermann M., et al., 2010b, ApJ, 712, 147  
 Ackermann M., et al., 2011, Phys. Rev. Lett., 107, 241302  
 Ackermann M., et al., 2012a, ApJ, 761, 91  
 Ackermann M., et al., 2012b, Phys.Rev., D85, 083007  
 Ackermann M., et al., 2013a  
 Ackermann M., et al., 2013b, Physical Review D 88., 082002  
 Ando S., 2009, Phy.Rev.D, 80, 023520  
 Ando S., Komatsu E., 2013, Phy.Rev.D, 87, 123539  
 Bringmann T., Weniger C., 2012, Physics of the Dark Universe, 1, 194  
 Cuoco A., Komatsu E., Siegal-Gaskins J. M., 2012, Phy.Rev.D, 86, 063004  
 Di Cintio A., Brook C. B., Macciò A. V., Stinson G. S., Knebe A., Dutton A. A., Wadsley J., 2014, MNRAS, 437, 415  
 Diemand J., Kuhlen M., Madau P., 2008, Astroph. J., 686, 262  
 Dutton A. A., Macciò A. V., 2014, In preparation.  
 Einasto J., 1965, Trudy Astrofizicheskogo Instituta Alma-Ata, 5, 87  
 Einasto J., 1969, Astrofizika, 5, 137  
 Fornasa M., Pieri L., Bertone G., Branchini E., 2009, Phys. Rev. D, 80, 023518  
 Fornasa M., Zavala J., Sánchez-Conde M. A., Siegal-Gaskins J. M., Delahaye T., Prada F., Vogelsberger M., Zandanel F., Frenk C. S., 2013, MNRAS, 429, 1529  
 Gomez-Vargas G. A., Sanchez-Conde M. A., Huh J.-H., Peiro M., Prada F., et al., 2013, JCAP10, 029  
 Górski K. M., Hivon E., Banday A. J., Wandelt B. D., Hansen F. K., Reinecke M., Bartelmann M., 2005, ApJ, 622, 759  
 Graham A. W., Merritt D., Moore B., Diemand J., Terzić B., 2006, AJ, 132, 2701  
 Harding J. P., Abazajian K. N., 2012, JCAP, 11, 26  
 Kutuzov S. A., Einasto J., 1968, Publications of the Tartu Astrofizika Observatory, 36, 341  
 Ludlow A. D., Navarro J. F., Angulo R. E., Boylan-Kolchin

- M., Springel V., Frenk C., White S. D. M., 2013, ArXiv e-prints
- Macciò A. V., Dutton A. A., van den Bosch F. C., 2008, MNRAS, 391, 1940
- Macciò A. V., Paduroiu S., Anderhalden D., Schneider A., Moore B., 2012, MNRAS, 424, 1105
- Macciò A. V., Stinson G., Brook C. B., Wadsley J., Couchman H. M. P., Shen S., Gibson B. K., Quinn T., 2012, ApJL, 744, L9
- Navarro J. F., Frenk C. S., White S. D. M., 1996, Astroph. J., 462, 563
- Navarro J. F., Frenk C. S., White S. D. M., 1997, ApJ, 490, 493
- Navarro J. F., Hayashi E., Power C., Jenkins A. R., Frenk C. S., White S. D. M., Springel V., Stadel J., Quinn T. R., 2004, MNRAS, 349, 1039
- Pieri L., Lavallo J., Bertone G., Branchini E., 2011, Phy.Rev.D, 83, 023518
- Ripken J., Cuoco A., Zechlin H.-S., Conrad J., Horns D., 2014, JCAP, 1, 49
- Sanchez-Conde M. A., Prada F., 2013, ArXiv e-prints
- Sefusatti E., Zaharijas G., Serpico P. D., Theurel D., Gustafsson M., 2014, ArXiv e-prints
- Siegal-Gaskins J. M., 2008, JCAP, 0810, 040
- Siegal-Gaskins J. M., Reesman R., Pavlidou V., Profumo S., Walker T. P., 2011, Mon.Not.Roy.Astron.Soc., 415, 1074S
- Springel V., Wang J., Vogelsberger M., Ludlow A., Jenkins A., Helmi A., Navarro J. F., Frenk C. S., White S. D. M., 2008, MNRAS, 391, 1685
- Stadel J., Potter D., Moore B., Diemand J., Madau P., Zemp M., Kuhlen M., Quilis V., 2009, MNRAS, 398, L21
- Stinson G. S., Brook C., Macciò A. V., Wadsley J., Quinn T. R., Couchman H. M. P., 2013, MNRAS, 428, 129
- Walker M., Combet C., Hinton J., Maurin D., Wilkinson M., 2011, Astrophys.J., 733, L46
- Xue X. X., Rix H. W., Zhao G., Re Fiorentin P., Naab T., Steinmetz M., van den Bosch F. C., Beers T. C., Lee Y. S., Bell E. F., Rockosi C., Yanny B., Newberg H., Wilhelm R., Kang X., Smith M. C., Schneider D. P., 2008, ApJ, 684, 1143